International Journal of Power Electronics and Drive System (IJPEDS)
Vol. 17, No. 1, March 2026, pp. 267~281
ISSN: 2088-8694, DOI: 10.11591/ijpeds.v17.i1.pp267-281

Modeling and analysis of batteryless off-grid photovoltaic with adaptive multi-motor

I Wayan Sutaya[1], Ida Ayu Dwi Giriantari[2], Wayan Gede Ariastina[2], I Nyoman Satya Kumara[2]
[1]Electronic Systems Engineering Technology, Universitas Pendidikan Ganesha, Singaraja, Indonesia
[2]Electrical Engineering, Universitas Udayana, Denpasar, Indonesia

Article Info

Article history:

Received Aug 11, 2025
Revised Oct 20, 2025
Accepted Dec 11, 2025

Keywords:

Batteryless
Model
Multi-motor
Photovoltaic
Power production

ABSTRACT

This paper presents a model of a batteryless off-grid photovoltaic (PV) system with an adaptive multi-motor load. This model is developed as an effort to enhance the power output of batteryless off-grid PV systems for motor loads. Instead of using a single large-capacity motor, as commonly done in previous studies, the model distributes the load into several smaller motors and controls them adaptively. This approach allows for better control of the total load impedance to support maximum power point (MPP) tracking. A case study involving three three-phase induction motors, each with an operating power of 200 W, is conducted, where the power production of the proposed model is analysed by comparing it with the theoretical MPP and a fixed-load motor system that represents a single large motor. Under 1000 W/m² irradiance and using an 852 Wp PV array, the proposed model achieves a power output of 842 W, which corresponds to 98.83% of the MPP. In contrast, the system without this model only generates 298 W, or just 35.02% of the MPP. The testing process spans a 5-second period during the motor starting state. The power production analysis of the proposed model is presented in graphical form using MATLAB/Simulink.

Corresponding Author:

I Wayan Sutaya
Electronic Systems Engineering Technology, Universitas Pendidikan Ganesha
Singaraja, Bali, Indonesia
Email: wsutaya@undiksha.ac.id

1. INTRODUCTION

The batteryless off-grid photovoltaic (PV) system is widely recognized as a practical application of PV technology, particularly suitable for supplying power to non-critical loads, as discussed in several studies [1]-[3]. These types of loads are characterized by their ability to operate only when energy is available, without relying on strict or continuous power demand requirements. Unlike conventional loads that must remain active based on user needs, these loads are only activated when sufficient solar energy is available to power them directly. Therefore, the batteryless off-grid PV system is highly suitable for flexible applications that can adapt to the naturally variable availability of renewable energy.

One of the practical applications of a batteryless PV system is as a power source for driving electric motor loads [4], [5]. This approach is employed for various purposes, including the operation of high-capacity water pumps that deliver water into reservoirs, distillation processes, and other mechanical applications that rely on motor-driven systems. In water pumping applications, the volume of water pumped is directly dependent on the intensity of solar irradiance. The higher the solar intensity, the greater the volume of water that can be delivered [6]. This process requires a control system capable of tracking the maximum power point (MPP), typically achieved by regulating the current supplied to the motor load [7].

In several studies, current control to the motor load is achieved by regulating the voltage supplied to the motor. This voltage regulation can be implemented using two main approaches: the single-stage method and the two-stage method. In the single-stage method, the system utilizes only an inverter block [8]-[13]. In contrast, the two-stage method employs both a converter and an inverter block in sequence [14]-[19]. The converter module is controlled using pulse width modulation (PWM) techniques, while the inverter is regulated based on the modulation index [20]. This control strategy is aimed at achieving MPP tracking, thereby optimizing the energy utilization from the PV system.

Studies generally regulate the voltage supplied to motor loads to track maximum power, with control applied through the inverter to manage current flow to the load [21], [22]. This is crucial because maximum power extraction depends heavily on achieving the optimal current level. However, challenges arise when the load is an electric motor, whose impedance varies with operating conditions and cannot be treated as a constant resistance [23]. The impedance value of the motor changes depending on its operating condition. During the starting phase, the impedance decreases significantly compared to the steady-state condition. Similarly, when the motor is loaded, its impedance also becomes lower. Conventional systems often use a single large motor or multiple motors connected statically in parallel, which may reduce control flexibility.

Due to the dynamic nature of motor loads [24], which differ significantly from conventional resistive loads, current control from the PV panel through voltage regulation alone is insufficient. An additional control variable is required to achieve more efficient maximum power tracking. One potential approach is to modify the motor load configuration itself by replacing a single large motor or multiple statically connected motors with an adaptive multi-motor load. This allows the number of operating motors to be controlled, making the total impedance of the motor loads a variable.

This paper presents a power production analysis of a model of a batteryless off-grid photovoltaic system with adaptive motor load, which was developed as part of the research conducted in this study. The proposed model aims to optimize power utilization from the PV system by adjusting the number of active motors based on the availability of solar energy. The findings demonstrate a significant improvement in power output compared to conventional approaches. Evaluation was conducted by measuring the system's power output at the MPP under varying levels of solar irradiance. For comparison, tests were also performed on a fixed motor load configuration, representing systems with a single large motor or multiple statically operated motors. This comparison highlights the advantages of the adaptive load model in enhancing PV power utilization efficiency.

2. PV SYSTEM FOR MOTOR DRIVE APPLICATIONS

Photovoltaic (PV) panels generate electrical power based on the level of solar irradiance they receive [25], [26]. Each irradiance level corresponds to a specific maximum power that the PV can deliver. This maximum power can only be achieved when the output current and voltage of the PV meet the required conditions. If the current drawn is either lower or higher than the optimal value, the PV will fail to operate at its MPP [27], [28]. In this context, the characteristics of the motor load become a critical factor in determining the PV system's ability to reach and maintain maximum power production [29].

The PV system as a source of electrical energy is represented using an equivalent circuit model, as illustrated in Figure 1(a). In this model, the PV is considered as a current source. The MPP the PV can deliver is reflected in the behavior of this equivalent circuit. Under short-circuit conditions, as described in (1), the maximum current flows directly to the load. In contrast, under open-circuit conditions, the entire current flows through the diode component I_D, causing the forward-bias voltage to reach its peak value. Consequently, the terminal voltage also reaches its maximum level, as stated in (2). The current output from the PV during active load operation is shown in (3) [30], [31].

$$I_{sc} = I_{pv} - I_0 \left[exp\ \left(\frac{I_{sc}R_s}{aV_T} \right) - 1 \right] - \frac{I_{sc}R_s}{R_{sh}} \quad (1)$$

$$V_{OC} = \frac{nkT}{q} ln\ \left(\frac{I_L}{I_0} + 1 \right) \quad (2)$$

$$I_L = I_{PV} - I_0 \left(exp\ \left(\frac{qV + qR_SI}{NKT} \right) - 1 \right) - \left(\frac{V + R_SI}{R_{sh}} \right) \quad (3)$$

The induction motor load used to drive the pump exhibits power consumption characteristics that can be represented using an equivalent circuit model, as shown in Figure 1(b). The current flowing into the motor is determined by the output voltage of the inverter and the impedance of the motor itself. Several studies, such as that conducted by [32], have controlled the motor's input current by regulating the inverter

output voltage. Meanwhile, the motor impedance is defined by its resistance and reactance, which are typically not actively controlled but allowed to vary naturally during operation. The motor resistance is constant and can be determined in advance, whereas the reactance depends on the motor's operating conditions, particularly the slip, which varies continuously during operation [33], [34].

To date, no study has specifically highlighted the role of impedance in determining the magnitude of current flowing into the motor. This indicates a research gap that forms the basis for novelty in the present study. The impedance value reflects the overall performance characteristics of the motor load. Total impedance plays a crucial role in determining the stator input current and influences the motor's dynamic response, especially during transient conditions such as startup or load changes. The slip value (s) directly affects the motor impedance Z_{motor}, which in turn impacts both the current magnitude and the resulting electromagnetic torque [35], [36].

$$Z_{\text{motor}} = R_s + jX_s + \left(\frac{R_r'}{s} + jX_r'\right) \quad (4)$$

The treatment of the load side plays a critical role in determining the amount of power that can be produced by the PV panel. Each level of solar irradiance corresponds to a different MPP. To ensure that the PV operates at maximum power under varying irradiance conditions, the output current must align with the MPP current, I_{mp}. This current value varies with irradiance levels and is highly dependent on the characteristics of the connected load.

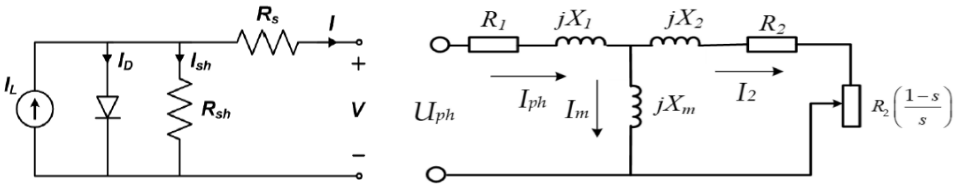

(a) (b)

Figure 1. Equivalent circuit of (a) photovoltaic system [30] and (b) induction motor [35]

3. METHOD

The model of batteryless off-grid photovoltaic system with adaptive motor load developed in this study is illustrated in Figure 2. The PV array supplies electrical power based on the received solar irradiance. In this model, each motor is connected in parallel with both the PV array and other motors. Each motor load is equipped with its own converter and inverter, which are controlled by a centralized control unit. This control unit manages the operation of each motor deciding whether it should be activated or not and determines the voltage level supplied to each motor load. Control is carried out by adjusting both the converter and inverter associated with each motor unit.

In various studies on batteryless PV systems for pump operation, the load impedance could not be actively controlled, as the system typically employed either a single large motor or multiple motors connected in a fixed configuration, effectively functioning as a single large load [37], [38]. In contrast, the proposed model in this study allows the equivalent impedance to be adjusted, resembling the behavior of a rheostat. This is made possible through the use of an adaptive multi-motor load, where the total load can be increased by activating additional motors.

$$(P_{\text{PV}} = P_{\text{motor}}) \quad (5)$$

$$(V_{\text{PV}} \cdot I_{\text{PV}} = \sqrt{3} \cdot V_{\text{ph}} \cdot I_{\text{ph}} \cdot \cos\theta) \quad (6)$$

$$(P_{\text{motor}} = \frac{\sqrt{3} \cdot V_{\text{ph}}^2}{Z_{\text{motor}}} \cdot \cos\theta) \quad (7)$$

$$Z_{\text{motor}} = \left(\sum_{k=1}^{n} \frac{1}{R_s + \frac{R_{r_k}'}{s} + j\left(X_s + X_{r_k}'\right)}\right)^{-1} \quad (8)$$

The power generated by the PV panel is calculated based on the relationship described in (5)-(7) where Z_{motor} represents the impedance of the motor [39]. This approach limits the system's flexibility in

adapting to variations in solar irradiance. The proposed adaptive multi-motor model calculates the PV output current as the sum of the individual currents drawn by each motor, where each motor operates with its own voltage and impedance characteristics. By independently controlling the voltage for each motor and selectively activating or deactivating motors as needed, the system can dynamically adjust its total equivalent impedance, as formulated in (9). As a result, power production can more closely approach the MPP under varying irradiance conditions.

The proposed and tested model is illustrated in Figure 2. The multi-motor load in this configuration is represented using three three-phase motors. As the system implements a two-stage power conversion architecture, the regulation of electrical power consumption for each motor is achieved through both the converter and inverter modules. The converter module provides a DC output voltage, while the inverter module generates a three-phase AC output voltage.

The model developed in this study was simulated and tested using MATLAB, as illustrated in Figure 3. To represent the multi-motor load, three three-phase induction motors were used, each rated at 200 W. Each motor is equipped with its own converter and inverter circuitry, all connected to a centralized control unit. This control unit determines which motors should be activated by regulating their respective converters and inverters. Additionally, the control unit monitors the PV output current and implements the Perturb and Observe (P&O) method to track the MPP [40], [41].

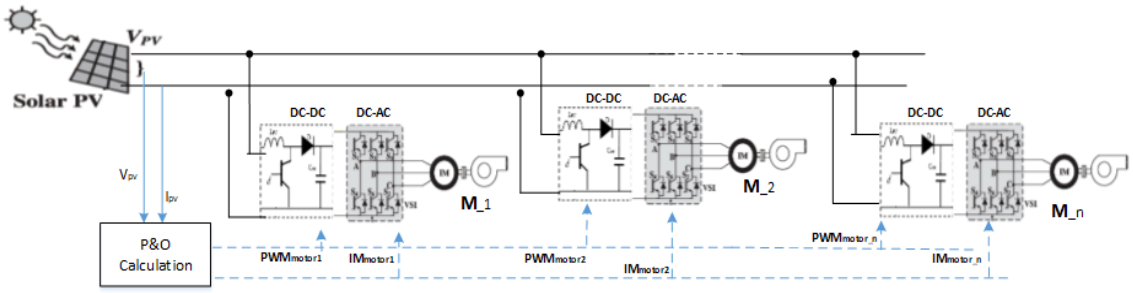

Figure 2. A model of a batteryless off-grid PV system with adaptive multi-motor load developed in this study

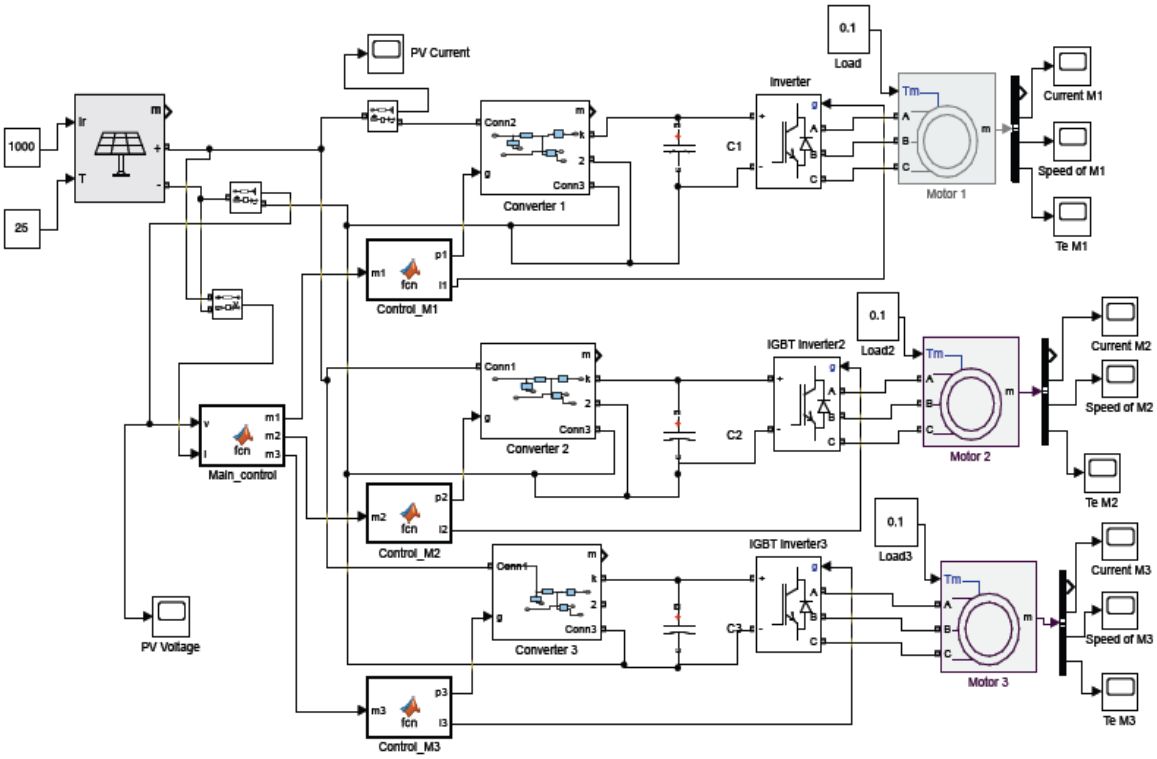

Figure 3. Design and testing of a model of a batteryless off-grid PV system with adaptive multi-motor load developed in this study using MATLAB

4. RESULTS AND DISCUSSION

In the testing and analysis process of the developed model, a PV array with a capacity of 852 Wp was used. Figure 4(a) presents the MPP curve of the PV under various levels of solar irradiance. The maximum power output of 852 W was achieved when the solar panel received an irradiance of 1000 W/m², with an output current of 7.35 A. Under this condition, the PV output voltage adjusted to approximately 116 V. Meanwhile, Figure 4(b) shows the current-voltage (I–V) characteristics, illustrating how the PV voltage varies with changes in the output current.

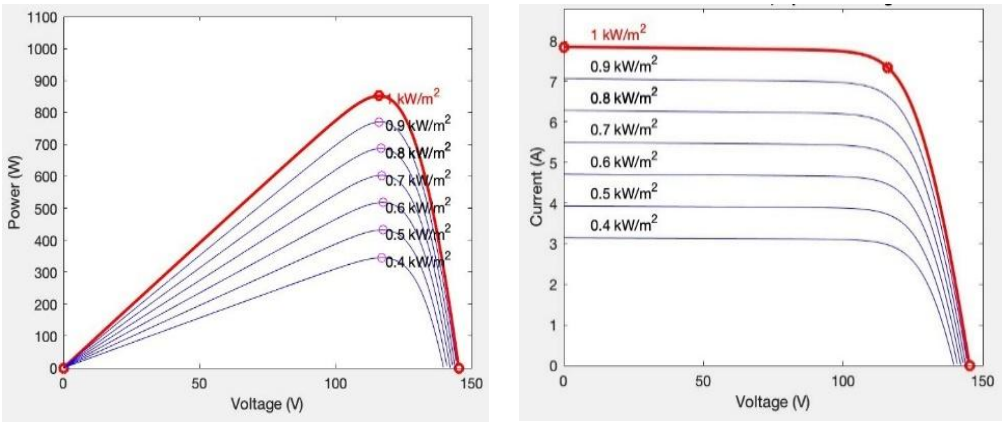

(a) (b)

Figure 4. Power production graphs: (a) power output versus voltage and (b) current output from the PV versus voltage at the PV terminal

4.1. PV power output and motor load consumption results

The simulation test results of PV power production and motor power consumption, along with the performance of the motor loads, are presented in the form of graphs. These graphs display the current drawn by each motor load. Oscillations in the current are observed as the motors reach their steady-state condition, which is caused by the oscillating electromagnetic force generated by the motors that opposes the incoming current. During the starting condition, the motors have not yet reached their maximum speed, resulting in a relatively small back electromotive force (EMF) [23]. From the test result graphs, the time required by each motor to reach steady-state conditions can be clearly observed.

4.1.1. Irradiance of 1000 W/m² with adaptive multi-motor load

The current consumption graph under an irradiance condition of 1000 W/m² is shown in Figure 5. In Figure 5(a), the current drawn by Motor 1 during the initial starting condition is recorded at 7.3 A. Within approximately 0.7 seconds, Motor 1 reaches its steady-state condition, resulting in a significant reduction in current to 1.9 A. After Motor 1 reaches steady state, Motor 2 is activated. The starting current drawn by Motor 2 is 5.5 A, and it reaches a steady-state condition in about 0.9 seconds, as presented in Figure 5(b). Next, in Figure 5(c), Motor 3 is turned on with a starting current of 4 A and reaches a steady-state condition within 1.25 seconds. Once all three motors have reached steady-state operation, each draws approximately the same current, around 1.8 A.

The total time required to reach steady-state conditions for the entire system is 2.85 seconds. This value is obtained by measuring the peak current consumption during the starting process until all three motors reach steady-state. Based on Figure 5(d), the total current drawn when all three motors are in steady-state operation is 7.47 A. This value is very close to the current at the MPP, which is 7.35 A.

The power consumption graph of the motor loads under 1000 W/m² irradiance is shown in Figure 6. In Figure 6(a), the power consumed by Motor 1 during the starting condition reaches 847 W over a period of 0.7 seconds. After reaching steady-state, the power consumption of Motor 1 drops significantly to around 200 W. Once Motor 1 is in steady-state, Motor 2 is then activated, as presented in Figure 6(b), consuming 650 W for approximately 0.9 seconds before stabilizing. Subsequently, in Figure 6(c), Motor 3 is switched on, drawing 500 W during its starting phase and requiring about 1.25 seconds to reach steady-state. Overall, the graph illustrates the power consumption characteristics of each motor from the starting phase to the steady-state condition.

The total time required to reach the steady-state condition is 2.85 seconds. The power produced by the PV system to bring the three motors into steady-state operation is 842 W, as shown in Figure 6(d). This power level is already very close to the MPP, which is 852 W. This indicates that the PV system operates efficiently, delivering nearly maximum available power during the steady-state condition of the multi-motor load.

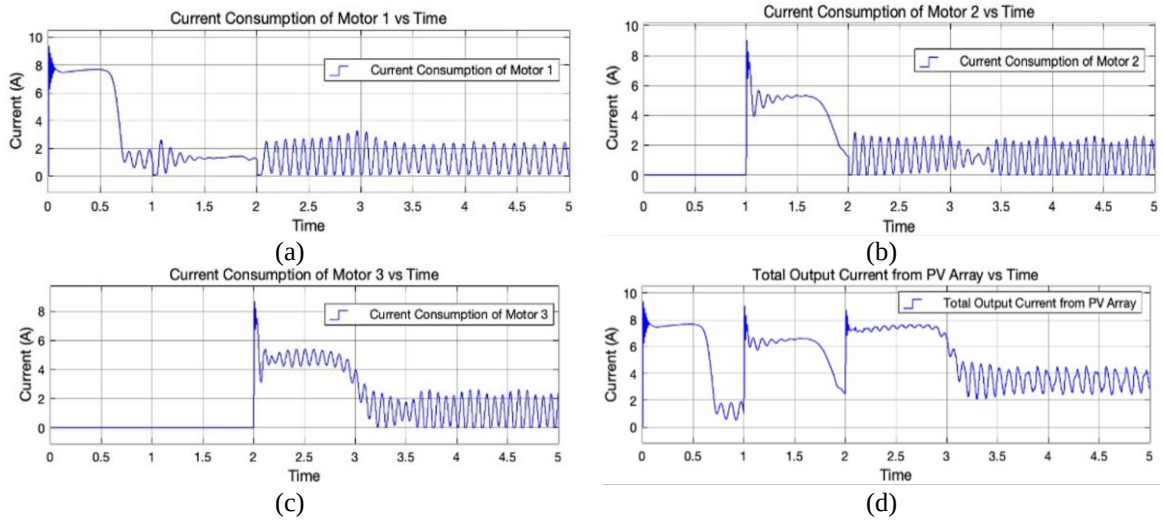

Figure 5. Current flow to motor loads under 1,000 W/m² irradiance: (a) current flowing to Motor 1 load, (b) current flowing to Motor 2 load, (c) current flowing to Motor 3 load, and (d) total current output from the PV

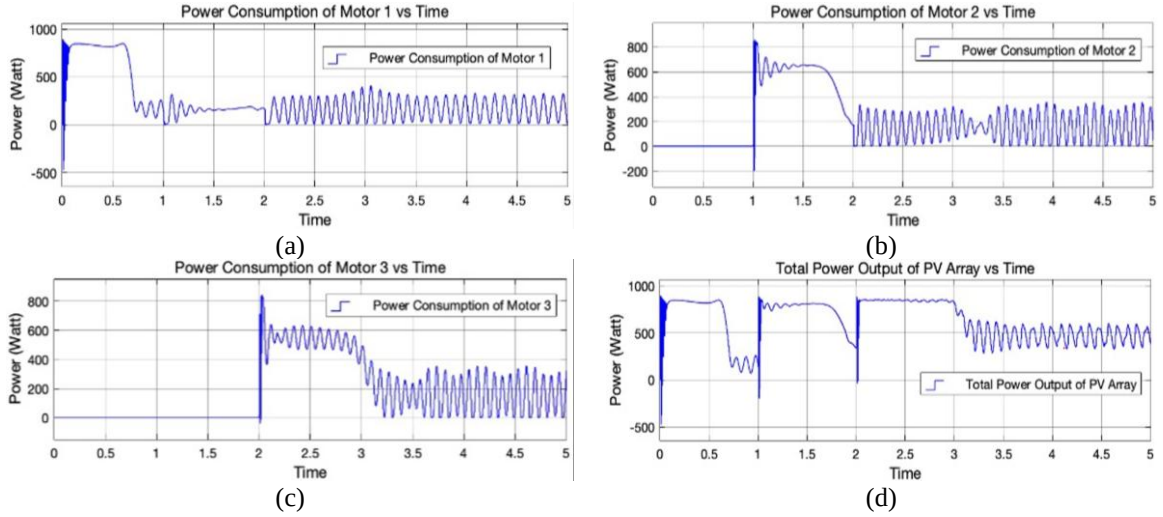

Figure 6. Power consumption by motor loads under 1000 W/m² irradiance: (a) power consumed by Motor 1 load, (b) power consumed by Motor 2 load, (c) power consumed by Motor 3 load, and (d) power produced by PV

The motor speed graph, used as an indicator of the steady-state condition of the motor loads under 1000 W/m² irradiance, is shown in Figure 7. The maximum motor speed of 1500 rpm is achieved at steady-state. This speed also serves as an indicator that the motor has reached its steady operating condition. In Figure 7(a), Motor 1 takes 0.7 seconds to reach steady-state. In Figure 7(b), Motor 2 requires 0.9 seconds, while in Figure 7(c), Motor 3 takes 1.25 seconds to reach steady-state. Figure 7(d) shows the voltage at the PV terminal.

4.1.2. Irradiance of 900 W/m² with adaptive multi-motor model

When the PV receives irradiance of 900 W/m², Motor 1 is activated first until it reaches steady-state. The current flowing to Motor 1 during the transition to steady-state is shown in Figure 8(a). It can be seen that a current of 6.8 A flows to Motor 1 for 0.8 seconds. After that, Motor 1 reaches steady-state and draws a

smaller current of 1.8 A. Next, as shown in Figure 8(b), Motor 2 is activated, drawing a current of 4.9 A for 1 second. Subsequently, in Figure 8(c), Motor 3 is turned on, drawing 3.2 A and requiring 2.5 seconds to reach steady-state. The graph of the current output from the PV is shown in Figure 8(d).

The total time required for all motors to reach steady-state is 4.3 seconds. The current drawn to bring the three motors into steady-state operation is 6.7 A, as shown in Figure 8(d). This current value is very close to the MPP current, which is 6.62 A.

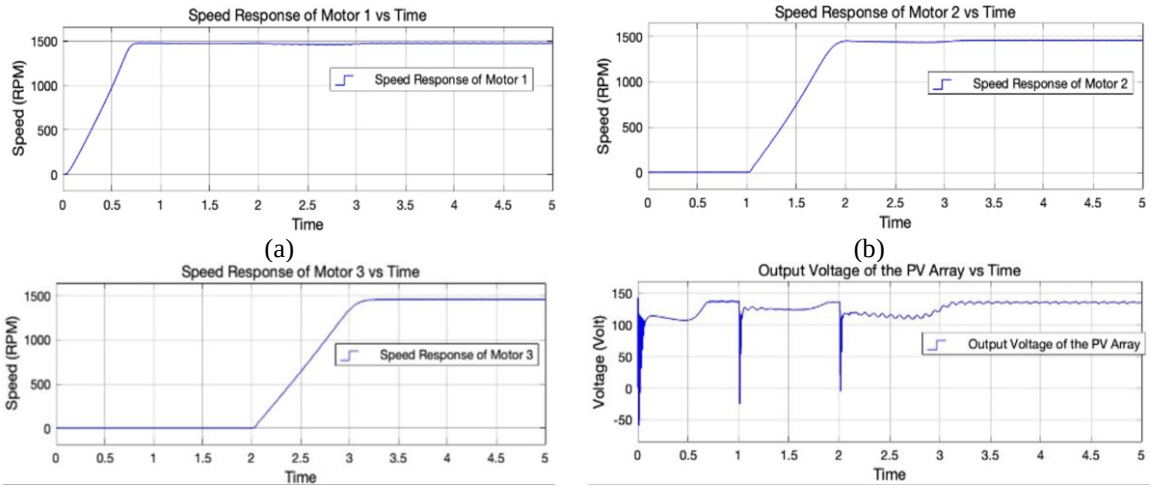

Figure 7. Irradiance of 1000 W/m² with PWM 30 and modulation index 0.85: (a) Motor 1 speed reaching steady-state, (b) Motor 2 speed reaching steady-state, (c) Motor 3 speed reaching steady-state, and (d) voltage at the PV terminal

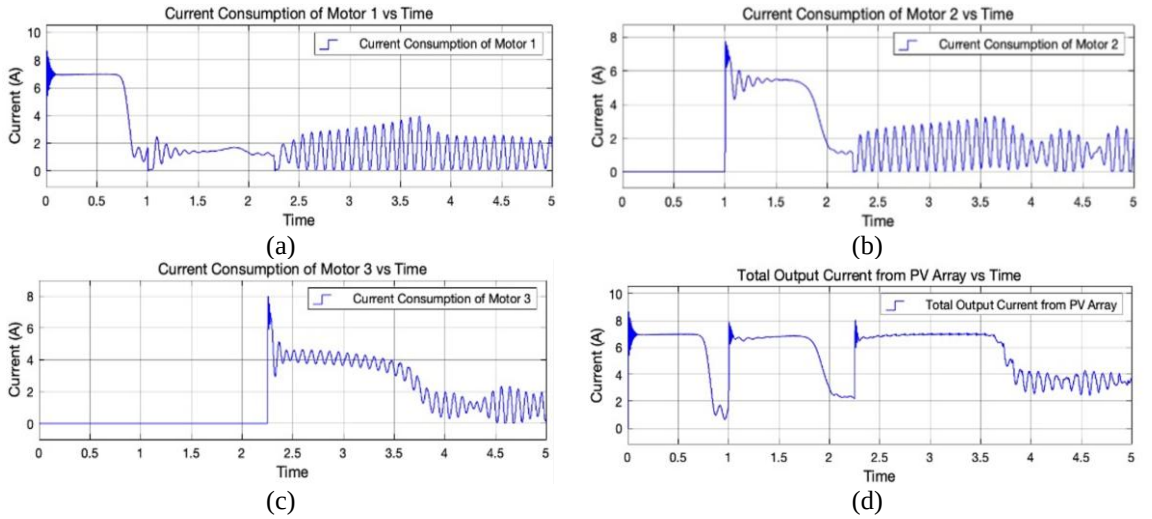

Figure 8. Current flow to motor loads under 900 W/m² irradiance with adaptive multi-motor configuration: (a) current in Motor 1, (b) current in Motor 2, (c) current in Motor 3, (d) total current from the PV

The power consumption of the motor loads under an irradiance level of 900 W/m² is illustrated in Figure 9. As shown in Figure 9(a), Motor 1 consumes 761 W during the starting-state condition, which lasts for approximately 0.8 seconds. After reaching steady-state, its power consumption decreases significantly to 200 W. Under this condition, Motor 2 is then activated, drawing 562 W for about 1 second, as shown in Figure 9(b). Subsequently, Motor 3 is switched on and consumes 360 W during its starting-state condition. Motor 3 requires approximately 2.5 seconds to reach steady-state, as depicted in Figure 9(c). The total maximum power that can be produced, 760 W, is presented in Figure 9(d).

The average power generated by the PV system to bring the three motor loads to steady-state condition is 760 W. Meanwhile, the MPP of the PV under an irradiance level of 900 W/m² is 765 W. This

indicates that the power produced by the PV is very close to its maximum power point, demonstrating that the adaptive multi-motor load model operates efficiently and optimally in utilizing the available power.

The graph illustrating the speed of each motor load is shown in Figure 10. The motor speed graph serves as an indicator of when each motor reaches the steady-state condition. Steady-state is achieved when the motor reaches a speed of 1500 rpm. The figure displays the speed profile of each motor as it approaches steady-state. Respectively, Figures 10(a)-10(c) show the ability of Motor 1, Motor 2, and Motor 3 to reach steady-state conditions within 0.8 s, 1.0 s, and 1.5 s. Meanwhile, Figure 10(d) presents the output voltage of the PV system.

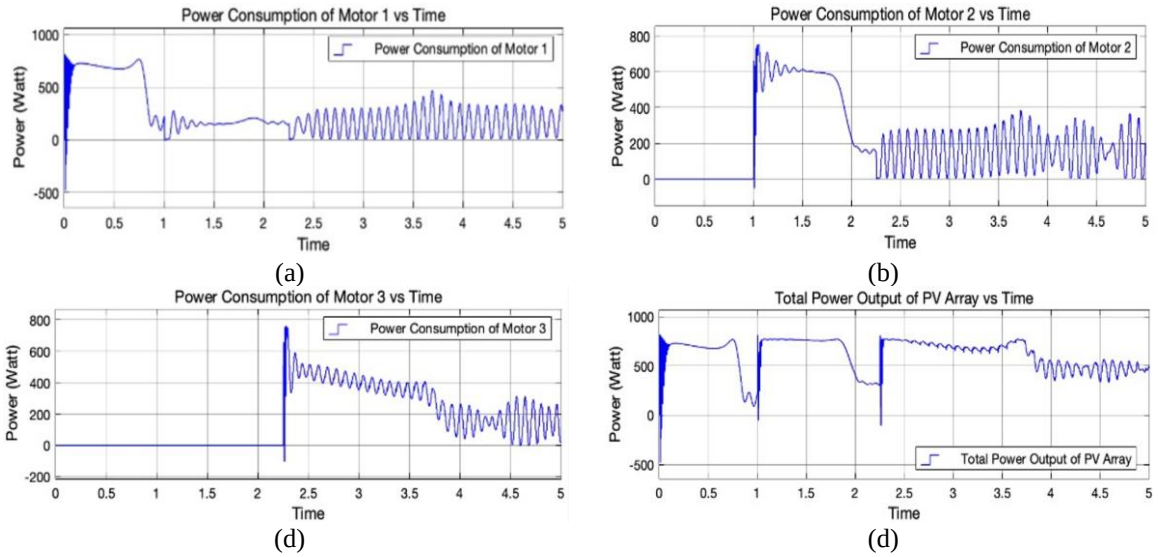

Figure 9. Power consumption by motor loads under 900 W/m² irradiance: (a) power consumed by Motor 1 load, (b) power consumed by Motor 2 load, (c) power consumed by Motor 3 load, and (d) total power produced by the PV

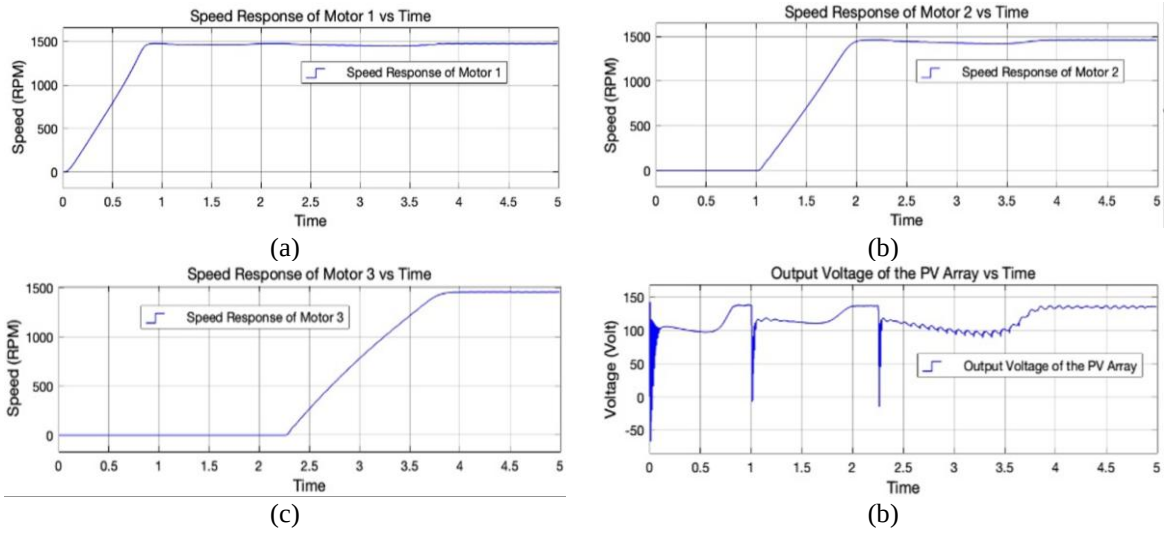

Figure 10. Motor load speed under 900 W/m² irradiance: (a) speed of Motor 1 load, (b) speed of Motor 2 load, (c) speed of Motor 3 load, and (d) PV output voltage

4.1.3. Irradiance of 1000 W/m² with fixed multi-motor configuration

As a comparison to the performance of the adaptive multi-motor load model developed in this study, a test was also conducted using a fixed multi-motor configuration with the same load. This type of load serves as a representation of the study presented in [4], [5]. In this scenario, the three motor loads were

connected in a fixed manner without employing an adaptive control system. This configuration can also be considered as a representation of a single large motor with an equivalent total power rating.

Figure 11 illustrates the current consumption of each motor and the total current output from the PV under the fixed configuration. Figures 11(a)–11(c) illustrate that Motors 1, 2, and 3 consume the same current of 2.59 A. Figure 11(d) illustrates that the total current drawn by the three motors is 7.77 A, whereas the ideal current required for the PV to operate at its maximum power point (MPP) is 7.35 A. This discrepancy indicates that the PV system is not operating at its maximum power point, leading to suboptimal utilization of the available power. As a result, the overall efficiency of the PV system in this configuration is reduced.

Figures 12(a)-12(c) illustrate that each motor consumes 99 W, resulting in a total power consumption of 298 W, as presented in Figure 12(d). This value is significantly lower than the maximum capacity of the PV, which is capable of delivering up to 852 W at the MPP. During the 5-second simulation, all motors remained in the starting condition, and none of them reached the steady-state condition. This outcome indicates that the fixed multi-motor configuration is unable to utilize the available power from the PV effectively, resulting in inefficient overall system performance.

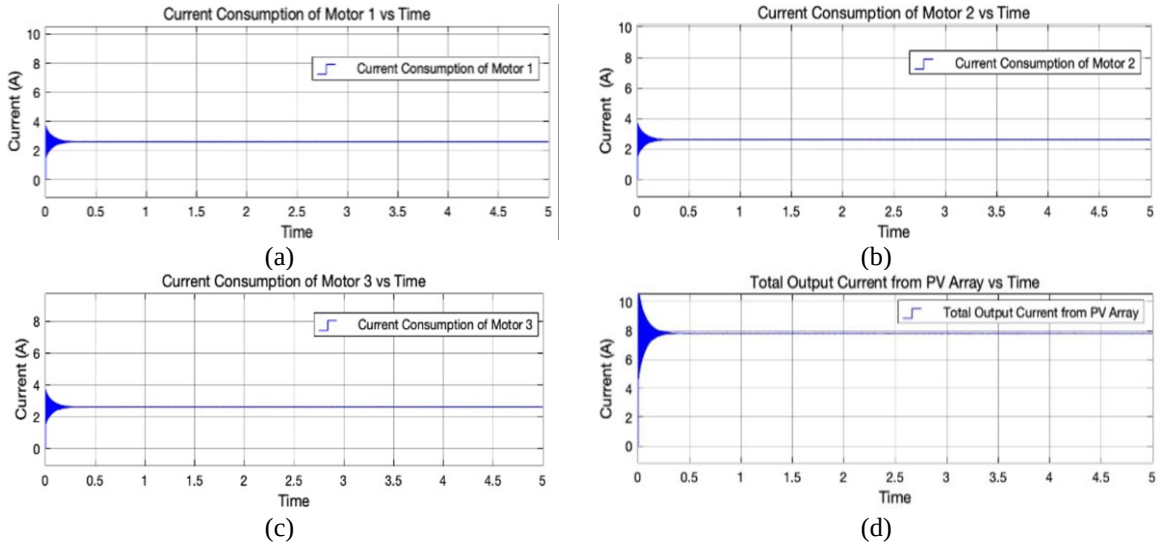

Figure 11. Current flow to motor loads under 1,000 W/m² irradiance with statically connected motor loads: (a) current in Motor 1, (b) current in Motor 2, (c) current in Motor 3, and (d) total current from the PV

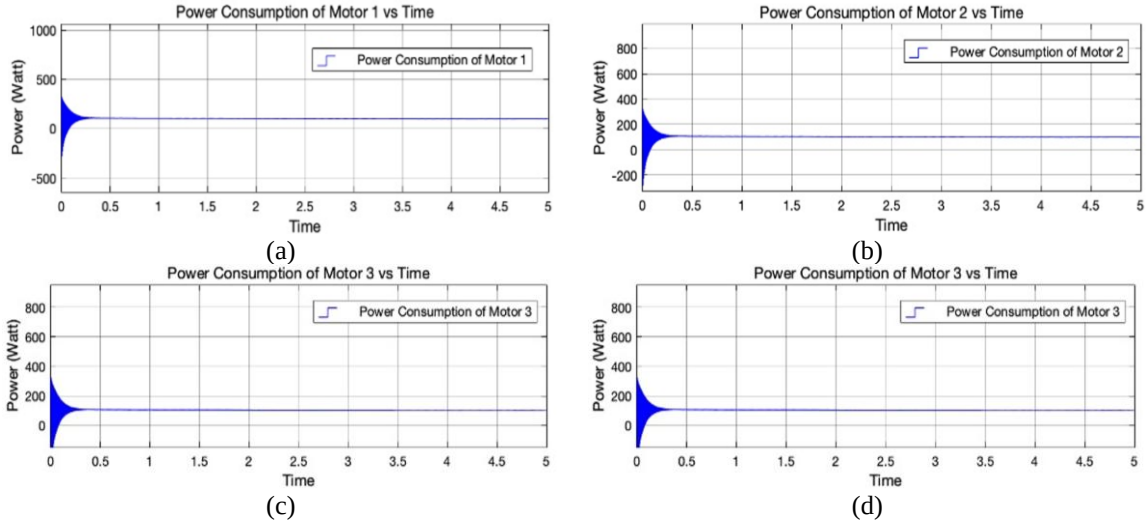

Figure 12. Irradiance of 1000 W/m² with statically connected motor loads (a) power consumed by Motor 1 load, (b) power consumed by Motor 2 load, (c) power consumed by Motor 3 load, and (d) total power produced by the PV

The motor speed resulting from the fixed multi-motor configuration, used as a comparison to the adaptive multi-motor load model, is shown in Figure 13. Based on the simulation results, the maximum speed achieved by each motor was only 500 rpm, as illustrated in Figures 13(a)–13(c), which is significantly lower than the expected steady-state speed of 1500 rpm. This indicates that the motors failed to reach the steady-state condition during the simulation period. Figure 13(d) shows the PV output voltage, which is notably low. This voltage drop was caused by the high current drawn simultaneously by all three motors. The total current exceeded the optimal current at the MPP, preventing the PV from operating efficiently. As a result, the system's overall efficiency was significantly reduced [42].

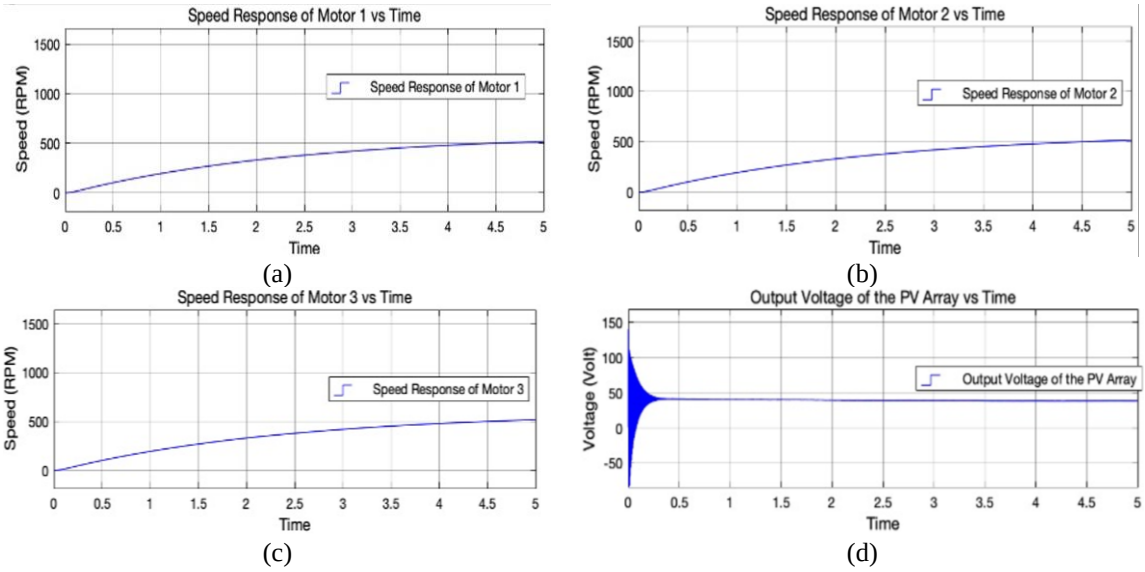

Figure 13. Irradiance of 1000 W/m² with statically connected motor: (a) speed of Motor 1, (b) speed of Motor 2, (c) speed of Motor 3, and (d) output voltage at the PV terminal

4.2. Analysis of test data results

Table 1 provides reference values for PV power output at the maximum power point under different levels of solar irradiance. For the PV module used in this study, rated at 852 Wp, the system delivers 852 W of power under an irradiance of 1000 W/m², assuming a load current of 7.5 A. At 900 W/m², the PV produces 765 W when the load draws 7 A of current, and so forth for other irradiance levels. The data in this table serve as a reference for evaluating the performance of the model of a batteryless off-grid PV system with adaptive multi-motor load developed in this study.

The measurement results from the overall power production test using the model of a batteryless off-grid PV system with adaptive multi-motor load are presented in Table 2. For the power production analysis under an irradiance level of 1000 W/m², the PV produced an average power output of 842 W. This value represents the average power required during the operation to bring the three motors to steady-state conditions. When all three motors were in the starting condition, Motor 1 received power (Pm1) of 847 W, Motor 2 (Pm2) received 643 W, and Motor 3 (Pm3) received 440 W. It is noted that each motor consumes 200 W when operating in a steady state. Based on the 5-second test duration, Motor 1 reached steady state in 0.7 seconds, while Motor 2 and Motor 3 required 0.9 seconds and 1.25 seconds, respectively.

The next analysis focuses on the measurement results under an irradiance level of 900 W/m². The power generated by the PV (Ppv) was 765 W. During the 5-second test duration, all motor loads were able to reach the steady-state condition. In this strategy, Motor 1 was set to consume 765 W of power, while the subsequent motor loads consumed 562 W and 360 W, respectively. Each motor consumes 200 W when operating in a steady state. The total time required for all motors to reach the steady-state condition was 3.3 seconds.

At the lowest irradiance level of 400 W/m², the PV system was able to generate 200 W of power. Under this condition, the system could only operate a single motor load. The system managed to regulate the power consumption of Motor 1 during the starting state by supplying it with 200 W equivalent to the power typically consumed in the steady-state condition. However, in this case, the power was controlled so that Motor 1 consumed 200 W from the beginning of the starting state. As a result, Motor 1 was able to reach steady state within 5 seconds.

Table 1. PV power production at the maximum power point

Irradiance	I_{mp} (A)	V_{mp} (V)	Pmp (W)	Isc (A)	Ioc (V)
1000	7.35	116	852.6	7.8	145.2
900	6.62	115.6	765.7	7.0	144.7
800	5.88	115.2	677.8	6.2	144.3
700	5.15	114.8	590.8	5.4	143.8
600	4.41	114.4	504	4.7	143.4
500	3.68	114	419.5	3.9	143.0
400	2.94	113.5	333.7	3.1	142.5

Table 2. PV power production in a model of batteryless off-grid PV system with adaptive multi-motor load

Irradiance (W/m^2)	I_{PV} (A)	V_{PV} (V)	Im1 (A)	Im2 (A)	Im3 (A)	Pm1 (W)	Pm2 (W)	Pm3 (W)	Ppv (W)	Tm1 (s)	Tm2 (s)	Tm3 (s)
1000	7.47	112.7	7.3	5.6	4	847	643	440	842	0.7	0.9	1.25
900	6.7	113.4	6.8	4.9	3.2	761	562	360	760	0.8	1.0	1.5
800	5.98	110.5	6.1	4.2	2.3	650	455	270	661	1	1.2	2
700	5.19	101.5	5.3	3.4	1.7	500	310	150	527	1.4	1.8	na
600	4.85	80.0	4.8	3.1	0	380	200	0	390	2.4	2.6	na
500	3.5	68.6	4	2.2	0	200	180	0	240	3.7	na	na
400	3.0	66.6	3.0	0	0	200	0	0	200	5	na	na

As a comparison to the power production performance of the adaptive model developed in this study, a test and analysis were also conducted on a PV system with fixed motor loads, as presented in Table 3. In the 5-second test under an irradiance level of 1000 W/m², the PV system was only able to produce 298 W of power. This amount of power was insufficient to bring the motor loads to the steady state, causing all motors to remain in the starting state throughout the entire test duration.

Since all three motor loads were connected in a fixed configuration and activated simultaneously, the system effectively operated as a single large load. As a result, the current drawn exceeded the optimal current at the PV's maximum power point, and the power generated was significantly lower than the maximum available power of 852 W under that irradiance level. This outcome demonstrates that the fixed multi-motor approach is inefficient in utilizing the available power from the batteryless off-grid PV system.

As a reference, the PV power production data at various irradiance levels are presented in Table 1, while the power output results for the adaptive model and the fixed configuration are shown in Tables 2 and 3, respectively. A comparison of these three scenarios is visualized in the graph in Figure 14(a). The graph clearly illustrates that the adaptive model is capable of producing power that closely approaches the PV's maximum power point, whereas the fixed configuration consistently yields power well below the PV's optimal capacity. This highlights the superiority of the adaptive load control strategy in enhancing the performance of batteryless PV systems.

At an irradiance level of 1000 W/m², the proposed system in this study operates very close to the maximum power point. As the irradiance level decreases, the PV power output slightly deviates from the maximum power point. This is due to the limited available power, which is only sufficient to operate a small number of motors, making it increasingly difficult to control the load precisely to match the optimal operating point. In comparison, without the adaptive model, the PV power output remains significantly low and far from the maximum power point across all irradiance levels.

In the 5-second test, without the use of the adaptive load model, none of the motors were able to reach the steady-state condition, despite steady state being essential for motors to operate normally. In contrast, with the implementation of the adaptive model, the motors were able to reach operational conditions more quickly compared to the fixed configuration, as illustrated in Figure 14(b). This figure shows that under an irradiance level of 1000 W/m², three motors successfully reached the steady state. Meanwhile, at 400 W/m², only one motor was able to achieve steady-state operation.

Table 3. PV power production in a static configuration

Irradiance (W/m^2)	I_{PV} (A)	V_{PV} (V)	Im1 (A)	Im2 (A)	Im3 (A)	Pm1 (W)	Pm2 (W)	Pm3 (W)	Ppv (W)	Tm1 (s)	Tm2 (s)	Tm3 (s)
1000	7.7	38.7	2.6	2.6	2.6	99.3	99.3	99.3	298.1	na	na	na
900	7.0	35.2	2.3	2.3	2.3	82.2	82.2	82.2	246.8	na	na	na
800	6.2	32.0	2.0	2.0	2.0	66.3	66.3	66.3	199	na	na	na
700	5.4	28.7	1.8	1.8	1.8	51.7	51.7	51.7	155	na	na	na
600	4.5	25.7	1.5	1.5	1.5	38.7	38.7	38.7	116	na	na	na
500	3.9	12.1	1.3	1.3	1.3	27.5	27.5	27.5	82.4	na	na	na
400	3.0	17.9	1.0	1.0	1.0	17.9	17.9	17.9	53.9	na	na	na

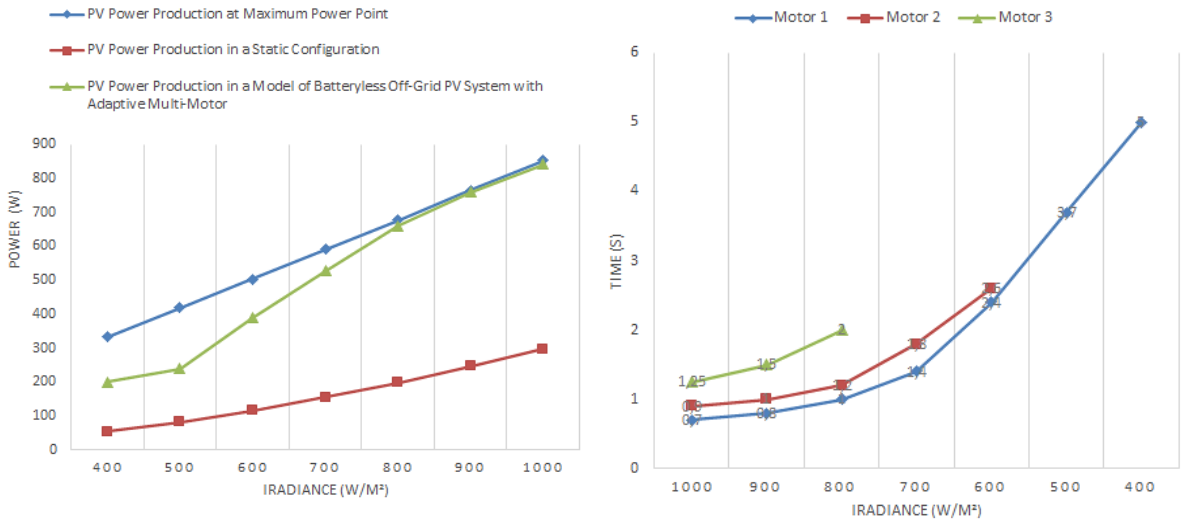

(a) (b)

Figure 14. Comparison graphs: (a) comparison of power production and (b) motor performance in reaching steady-state conditions

5. CONCLUSION

The batteryless off-grid PV system for motor loads represents an effort to supply flexible loads. In this system, the performance of the motor load is adapted to the amount of electrical power that can be generated by the PV. The main challenge lies in ensuring that the PV operates near its maximum power point, despite the inherently inconsistent and nonlinear characteristics of motor loads. Voltage control alone, as part of the maximum power point tracking process, is insufficient due to the load's nonlinear behavior. Therefore, a complementary load-side control strategy is required to appropriately manage the effective load value.

This study presents a model of a batteryless off-grid PV system with an adaptive multi-motor load. The proposed model introduces a mechanism to control not only the voltage supplied to the motors but also the effective load magnitude. This enables the PV system to consistently operate close to its maximum power point (MPP) under varying levels of solar irradiance. The load control strategy is realized by decomposing a single large motor load into multiple smaller motor units, which can be selectively and adaptively activated to match the available power, thereby optimizing energy utilization from the PV system.

The testing and analysis of the developed model, conducted through MATLAB simulations, demonstrated that the power output produced by the PV system closely approaches the maximum power point (MPP). This was verified by comparing the generated power at each irradiance level with the theoretical maximum power. The comparison was also extended to a conventional PV system without the adaptive model, which utilizes a fixed load configuration. This can be observed from the measurement results at an irradiance level of 1000 W/m², where the proposed model was able to produce 98.83% of the maximum power point, while the conventional model achieved only 35.02%.

The model developed in this study has successfully enabled motor loads to operate by allowing the motors to reach steady-state conditions more rapidly. From the tests conducted within a 5-second time span, the proposed model was able to operate three motors in steady-state conditions, whereas the conventional model failed to operate even a single motor. Therefore, the proposed model is highly suitable for batteryless off-grid PV systems. The power generated by the PV can be effectively utilized in a short time through the proposed system. This model can be adopted for various large-scale industrial applications that rely on electric motors for tasks requiring unrestricted operation.

ACKNOWLEDGMENTS

The authors gratefully acknowledge the technical support provided by The Center for Community Based Renewable Energy (CORE) at Udayana University, which enabled the timely completion of this research.

FUNDING INFORMATION

The authors gratefully acknowledge the financial assistance provided for conducting the research, authorship, and publication of this article, which was supported by the Ministry of Higher Education, Science, and Technology (Kemdiktiksainstek).

AUTHOR CONTRIBUTIONS STATEMENT

This journal uses the Contributor Roles Taxonomy (CRediT) to recognize individual author contributions, reduce authorship disputes, and facilitate collaboration.

Name of Author	C	M	So	Va	Fo	I	R	D	O	E	Vi	Su	P	Fu
I Wayan Sutaya	✓	✓	✓	✓	✓		✓	✓	✓	✓	✓		✓	✓
Ida Ayu Dwi Giriantari	✓	✓		✓	✓	✓		✓		✓		✓		✓
Wayan Gede Ariastina	✓	✓		✓	✓	✓		✓		✓		✓		✓
I Nyoman Satya Kumara	✓	✓		✓	✓	✓		✓		✓		✓	✓	✓

C : **C**onceptualization
M : **M**ethodology
So : **So**ftware
Va : **Va**lidation
Fo : **Fo**rmal analysis
I : **I**nvestigation
R : **R**esources
D : **D**ata Curation
O : Writing - **O**riginal Draft
E : Writing - Review & **E**diting
Vi : **Vi**sualization
Su : **Su**pervision
P : **P**roject administration
Fu : **Fu**nding acquisition

CONFLICT OF INTEREST STATEMENT

Authors state no conflict of interest.

DATA AVAILABILITY

The data that support the findings of this study, including MATLAB simulation files and results, are available from the corresponding author upon reasonable request.

REFERENCES

[1] Z. M. Dalala, S. Z. Alaqbani, D. R. Khirfan, L. H. Alhamad, M. Al-Addous, and N. Barbana, "Analysis and design methodology of a novel integration topology of storageless off-grid PV systems," *Energies*, vol. 15, no. 4, pp. 1–18, 2022, doi: 10.3390/en15041279.

[2] W. Khiari, M. Turki, and J. Belhadj, "Power control strategy for PV/Wind reverse osmosis desalination without battery," *Control Engineering Practice*, vol. 89, pp. 169–179, 2019, doi: 10.1016/j.conengprac.2019.05.020.

[3] A. Elnozahy, M. Abdel-Salam, and F. K. Abo-Elyousr, "Optimal techno-economic energy coordination of solar PV water pumping irrigation systems," *Energy*, vol. 288, 2024, doi: 10.1016/j.energy.2023.129817.

[4] B. Singh and R. Kumar, "Solar PV array fed brushless DC motor driven water pump," in *Proceedings IEEE 6th International Conference Power Systems (ICPS)*, 2016, pp. 1–4, doi: 10.1109/ICPES.2016.7584057.

[5] I. Saady, M. Karim, B. Bossoufi, N. El Ouanjli, S. Motahhir, and B. Majout, "Optimization and control of photovoltaic water pumping system using Kalman filter based MPPT and multilevel inverter fed DTC-IM," *Results in Engineering*, vol. 17, p. 100829, 2023, doi: 10.1016/j.rineng.2022.100829.

[6] H. H. Ammar, M. I. Mahmoud, A. T. Azar, and R. Shalaby, "An efficient design and control techniques of photo-voltaic pumping system (PVPS)," *Arabian Journal for Science and Engineering*, vol. 48, no. 11, pp. 14865–14882, 2023, doi: 10.1007/s13369-023-07861-2.

[7] M. Errouha, A. Derouich, N. El Ouanjli, and S. Motahhir, "High-performance standalone photovoltaic water pumping system using induction motor*," International Journal of Photoenergy*, vol. 2020, 2020, doi: 10.1155/2020/3872529.

[8] M. Abd El Sattar, K. Ahmed, A. AboZied, and A. Diab, "Adaptive MPPT of water photovoltaic pumping system based on vector controlled induction motor drives," *Journal of Advanced Engineering Trends*, vol. 41, no. 2, pp. 261–274, 2021, doi: 10.21608/jaet.2021.47871.1065.

[9] S. Shukla and B. Singh, "Single-stage pv-grid interactive induction motor drive with improved flux estimation technique for water pumping with reduced sensors," *IEEE Transactions on Power Electronics*, vol. 35, no. 12, pp. 12988–12999, 2020, doi: 10.1109/TPEL.2020.2990833.

[10] S. Shukla and B. Singh, "Single-stage PV array fed speed sensorless vector control of induction motor drive for water pumping," *IEEE Transactions on Industry Applications*, vol. 54, no. 4, pp. 3575–3585, 2018, doi: 10.1109/TIA.2018.2810263.

[11] Y. Biletskyi and I. Shchur, "Efficiency improvement in standalone solar PV water pumping system by pulsating pump operation based on intermediate supercapacitor buffer," *e-Prime - Advances in Electrical Engineering, Electronics and Energy*, vol. 11, 2025, doi: 10.1016/j.prime.2025.100913.

[12] V. Kumar and R. Agarwal, "Single stage transformerless multilevel inverter for solar PV application," *Computers & Electrical Engineering*, vol. 123, 2025, doi: 10.1016/j.compeleceng.2025.110243.

[13] G. Boztas, O. Aydogmus, and M. Yilmaz, "Optimized design of SynRM drive systems for high-efficiency solar water pumps," *Heliyon*, vol. 10, no. 20, p. e39478, 2024, doi: 10.1016/j.heliyon.2024.e39478.

[14] A. Narendra, V. Naik N, A. K. Panda, and R. K. Lenka, "Solar PV fed FSVSI based variable speed IM drive using ASVM Technique," *Engineering Science and Technology, an International Journal*, vol. 40, p. 101366, 2023, doi: 10.1016/j.jestch.2023.101366.
[15] T. Hamdi and A. Toumi, "Sliding mode controller with fuzzy supervisor for MPPT of Photovoltaic Pumping system," *International Journal of Power Electronics and Drive Systems (IJPEDS)*, vol. 14, no. 3, pp. 1639–1650, 2022, doi: 10.11591/ijpeds.v14.i3.pp1639-1650.
[16] S. Fahad, N. Ullah, A. J. Mahdi, A. Ibeas, and A. Goudarzi, "An advanced two-stage grid connected PV system: A fractional-order controller," *International Journal of Renewable Energy Research*, vol. 9, no. 1, pp. 504–514, 2019, doi: 10.20508/ijrer.v9i1.9031.g7609.
[17] R. Nisha and K. Gnana Sheela, "Review of PV fed water pumping systems using BLDC Motor," *Materials Today: Proceedings*, vol. 24, pp. 1874–1881, 2019, doi: 10.1016/j.matpr.2020.03.612.
[18] R. Kumar and M. V. Naik, "Robust soft computing optimized PWM-enhanced IFOC control for hybrid solar–fuel cell induction motor drives in water pumping systems," *International Journal of Hydrogen Energy*, vol. 137, pp. 538–552, 2025, doi: 10.1016/j.ijhydene.2025.05.047.
[19] Á. A. Orta-Quintana *et al*., "Robust two-stage controller for the bidirectional full-bridge Buck inverter–DC motor fed by renewable energy," *Results in Engineering*, vol. 26, p. 105209, 2025, doi: 10.1016/j.rineng.2025.105209.
[20] I. K. Wiryajati, I. A. D. Giriantari, I. N. S. Kumara, and L. Jasa, "The performance analysis of dual-inverter three phase fed induction motor with open-end winding using various PWM schemes," *Wireless Networks*, vol. 27, no. 2, pp. 871–880, 2021, doi: 10.1007/s11276-019-02182-5.
[21] N. Yussif, O. H. Sabry, A. S. Abdel-Khalik, S. Ahmed, and A. M. Mohamed, "Enhanced quadratic v/f-based induction motor control of solar water pumping system," *Energies*, vol. 14, no. 1, 2021, doi: 10.3390/en14010104.
[22] H. Chen and S. Ye, "Modeling of common-mode impedance of an inverter-fed induction motor from online measurement," *IEEE Transactions on Electromagnetic Compatibility*, vol. 60, no. 5, pp. 1581–1589, 2018, doi: 10.1109/TEMC.2017.2779886.
[23] M. Konuhova, "Modeling of induction motor direct starting with and without considering current displacement in slot," *Applied Sciences*, vol. 14, no. 20, 2024, doi: 10.3390/app14209230.
[24] M. Konuhova, "Induction motor dynamics regimes: a comprehensive study of mathematical models and validation," *Applied Sciences*, vol. 15, no. 3, 2025, doi: 10.3390/app15031527.
[25] A. M. Badea, D. Manaila-Maximean, L. Fara, and D. Craciunescu, "Maximizing solar photovoltaic energy efficiency: mppt techniques investigation based on shading effects," *Solar Energy*, vol. 285, p. 113082, 2025, doi: 10.1016/j.solener.2024.113082.
[26] M. Sravani and P. V. S. Sobhan, "Performance evaluation of solar PV integrated with custom power device under various load conditions," *e-Prime - Advances in Electrical Engineering, Electronics and Energy*, vol. 10, p. 100843, 2024, doi: 10.1016/j.prime.2024.100843.
[27] M. He, K. Zhou, Y. Xu, J. Yu, Y. Qu, and X. Wen, "An improved maximum power point tracking control scheme for photovoltaic systems," *Energies*, vol. 18, no. 12, 2025, doi: 10.3390/en18123182.
[28] K. I. Baradieh *et al.*, "Impact of different PV model parameters and various DC faults on the performance of photovoltaic arrays," *Inventions*, vol. 9, no. 5, 2024, doi: 10.3390/inventions9050093.
[29] S. Anbuchandran, D. S. Stephen, M. A. Babu, and A. Bhuvanesh, "MIWO-based MPPT of PV system for induction motor driven water pumping system," *e-Prime - Advances in Electrical Engineering, Electronics and Energy*, vol. 10, p. 100835, 2024, doi: 10.1016/j.prime.2024.100835.
[30] S. Faizan, A. L. I. Bukhari, U. Munir, and S. Ahmed, "Single phase induction motor fed water pump connected to photovoltaic generator," *International Journal of Industrial Electronics and Electrical Engineering*, vol. 7, no. 8, pp. 2347–2350, 2019.
[31] J. Meng, Q. Guo, M. Yue, and D. Diallo, "Comparative study of maximum power point tracking control for PV arrays system integration," *Control Engineering Practice*, vol. 147, 2024, doi: 10.1016/j.conengprac.2024.105906.
[32] S. Abbas and T. Iqbal, "Sensorless induction motor drive using coupled inductor based three phase inverters for solar pumping applications," *Results in Engineering*, vol. 26, p. 105300, 2025, doi: 10.1016/j.rineng.2025.105300.
[33] U. Sengamalai, G. Anbazhagan, T. M. T. Thentral, P. Vishnuram, T. Khurshaid, and S. Kamel, "Three phase induction motor drive: a systematic review," *Energies*, vol. 15, no. 21, 2022, doi: 10.3390/en15218260.
[34] A. Belgacem, Y. Miloud, M. Mostefai, and F. Belgacem, "Fuzzy logic direct torque control of induction motor for photovoltaic water pumping system," *International Journal of Power Electronics and Drive Systems (IJPEDS)*, vol. 13, no. 3, pp. 1822–1832, 2022, doi: 10.11591/ijpeds.v13.i3.pp1822-1832.
[35] M. Averbukh and E. Lockshin, "Estimation of the equivalent circuit parameters of induction motors by laboratory test," *Machines*, vol. 9, no. 12, 2021, doi: 10.3390/machines9120340.
[36] A. M. A. Hussain and H. M. D. Habbi, "Design and Performance Analysis of a 3-Phase Induction Motor for Solar Photovoltaic Fed Pumping System," *Journal of Engineering and Applied Sciences*, vol. 15, no. 3, pp. 773–782, 2019, doi: 10.36478/jeasci.2020.773.782.
[37] M. Errouha, S. Motahhir, and Q. Combe, "Twelve sectors DTC Strategy of IM for PV water pumping system," *Materials Today: Proceedings*, vol. 51, pp. 2081–2090, 2022, doi: 10.1016/j.matpr.2021.12.214.
[38] S. Dlimi *et al.*, "Modeling, Simulation and Efficiency Assessment of a Direct Coupled Water Pumping PV System," *Energy Conversion and Management: X*, vol. 23, 2024, doi: 10.1016/j.ecmx.2024.100626.
[39] H. Kraiem, "sensorless torque and flux control of induction motor fed by photovoltaic system," *Measurement and Control*, vol. 55, no. 5–6, pp. 454–462, 2022, doi: 10.1177/00202940221104869.
[40] V. H. Bui, V. D. Ha, V. A. Truong, and T. L. Duong, "A hybrid P&O and PV characteristics simulation method for GMPPT in PV systems under partial shading conditions," *Sensors*, vol. 25, no. 6, pp. 1–23, 2025, doi: 10.3390/s25061908.
[41] A. I. M. Ali and H. R. A. Mohamed, "Improved P&O MPPT algorithm with efficient open-circuit voltage estimation," *International Journal of Electrical Power & Energy Systems*, vol. 137, p. 107805, 2022, doi: 10.1016/j.ijepes.2021.107805.
[42] S. Chtita, A. Derouich, A. El Ghzizal, and S. Motahhir, "an improved control strategy for charging solar batteries in off-grid photovoltaic systems," *Solar Energy*, vol. 220, pp. 927–941, 2021, doi: 10.1016/j.solener.2021.04.003.

BIOGRAPHIES OF AUTHORS

I Wayan Sutaya is an academic member of the Faculty of Engineering and Vocational, Universitas Pendidikan Ganesha. He received a Bachelor of Engineering degree in Electrical Engineering from Udayana University in 2005 and a Master of Engineering degree in Electrical Engineering from the Bandung Institute of Technology in 2012. He has been serving as a lecturer in the Department of Electrical Engineering, Universitas Pendidikan Ganesha, since 2006. His research interests include renewable energy, electric drives, and power electronics. He can be contacted at email: wsutaya@undiksha.ac id.

Ida Ayu Dwi Giriantari is a professor in the Electrical Engineering Department, Udayana University, Indonesia, where she has been serving as a faculty member since 1991. She received the B.Eng. degree in electrical engineering from Udayana University in 1990, the M.Eng.Sc. degree in electrical engineering from the University of New South Wales (UNSW), Sydney, Australia, in 1999, and the Ph.D. degree in electric power from the same university in 2003, all under the sponsorship of the Indonesian Government. She is currently the Leader of the Center for Community-Based Renewable Energy (CORE) at Udayana University and a member of the Bali Center for Sustainable Finance (BCSF). Her research interests include renewable energy, energy management, photovoltaic systems, smart grids, high-voltage technology, and electric circuits. She is a Senior Member of IEEE and serves as a reviewer for various journals. She can be contacted at email: dayu.giriantari@unud.ac.id.

Wayan Gede Ariastina is a senior lecturer in the Electrical Engineering Department, Udayana University, Bali, Indonesia, where he has been a faculty member since completing his undergraduate degree in electrical engineering from the same university in 1994. He received the M.Eng.Sc. degree in electrical engineering from the University of New South Wales (UNSW), Sydney, Australia, in 1998, and the Ph.D. degree in electrical engineering from the same university in 2006, both supported by scholarships from the Indonesian Government. His research focuses on electrical energy management, green technology applications in electrical energy systems, and condition monitoring and diagnostics of power system equipment. He can be contacted at email: w.ariastina@unud.ac.id.

I Nyoman Satya Kumara is a faculty member in the Department of Electrical Engineering, Faculty of Engineering, Udayana University, Bali, Indonesia. He received his Bachelor of Engineering degree in Electrical Engineering from Udayana University in 1995, his Master of Science in Electrical Power from the University of Newcastle upon Tyne, United Kingdom, in 2000, and his Ph.D. in Electrical Engineering from the School of Electrical, Electronics, and Computer Engineering, University of Newcastle upon Tyne, in 2006. He has taught various subjects, including power electronics, electric drives, electrical energy conversion technology, renewable energy technology, smart grid, energy management, and English for electrical engineering. His research interests include electric drives, renewable energy, energy management, and smart systems. He can be contacted at email: satya.kumara@unud.ac.id.